

Atomic-resolution protein structure determination by cryo-EM

<https://doi.org/10.1038/s41586-020-2833-4>

Ka Man Yip¹, Niels Fischer¹, Elham Paknia¹, Ashwin Chari¹ & Holger Stark^{1,✉}

Received: 21 May 2020

Accepted: 14 September 2020

Published online: 21 October 2020

 Check for updates

Single-particle electron cryo-microscopy (cryo-EM) is a powerful method for solving the three-dimensional structures of biological macromolecules. The technological development of transmission electron microscopes, detectors and automated procedures in combination with user-friendly image processing software and ever-increasing computational power have made cryo-EM a successful and expanding technology over the past decade¹. At resolutions better than 4 Å, atomic model building starts to become possible, but the direct visualization of true atomic positions in protein structure determination requires much higher (better than 1.5 Å) resolution, which so far has not been attained by cryo-EM. The direct visualization of atom positions is essential for understanding the mechanisms of protein-catalysed chemical reactions, and for studying how drugs bind to and interfere with the function of proteins². Here we report a 1.25 Å-resolution structure of apoferritin obtained by cryo-EM with a newly developed electron microscope that provides, to our knowledge, unprecedented structural detail. Our apoferritin structure has almost twice the 3D information content of the current world record reconstruction (at 1.54 Å resolution³). We can visualize individual atoms in a protein, see density for hydrogen atoms and image single-atom chemical modifications. Beyond the nominal improvement in resolution, we also achieve a substantial improvement in the quality of the cryo-EM density map, which is highly relevant for using cryo-EM in structure-based drug design.

In recent years there has been rapid and exponential growth in the determination of high-resolution structures of macromolecular complexes by cryo-EM (https://www.ebi.ac.uk/pdbe/emdb/statistics_main.html), accompanied by a continuous shift in the highest attainable resolution of structures. Whereas the majority of the solved protein structures are still at resolutions of 3–4 Å, a growing number are in the 2–3 Å range, and a few are at a resolution better than 2 Å. The current record is a 1.54 Å resolution structure (EMD-9865) of apoferritin³. This structure was determined using a Jeol CryoARM 300 microscope equipped with a cold field emission gun electron source and an energy filter⁴. The increase in resolution raises important questions about the ultimate resolution limit of single-particle cryo-EM using existing electron microscope hardware. Here we use new hardware to determine the structure of the protein apoferritin at true atomic resolution, which enables the visualization of all atoms, including hydrogen atoms, in the protein.

New electron microscope hardware

We used a prototype instrument equipped with additional electron-optical elements to increase the performance of the electron microscope. A monochromator⁵ and a second-generation spherical aberration corrector⁶ (BCOR, CEOS GmbH) were built into a Titan Krios G3 (Thermo Fisher Scientific) electron microscope equipped with a Falcon 3 direct electron detector. This hardware combination

improved the optical properties by both reducing the energy spread of the electron beam (as a result of the monochromator) and reducing optical aberrations such as axial and off-axial coma (by the aberration corrector). As a reference, the microscope used here has an energy spread of about 0.1 eV, which is smaller than those of microscopes equipped with either Shottky field- or cold field-emission electron sources (approximately 0.7 eV or 0.4 eV, respectively); this provides increased temporal coherence and less dampening of high-resolution structural details in the images (Fig. 1). The additional BCOR spherical aberration corrector provides images that are free of axial and off-axial coma, which in the 1 Å-resolution regime is the most limiting aberration. In addition, the BCOR corrector can correct aberrations up to the fifth order and we use it to minimize linear magnification distortions in the images (Extended Data Fig. 1f). Linear magnification distortions are common in electron microscopy, and high-end microscopes suffer from these distortions typically in the relative range of 0.5–1%. Such values are negligible in attaining 3 Å-resolution structures for relatively small objects, but can become resolution-limiting for larger macromolecular complexes and/or when approaching atomic resolution. Typical linear magnification distortions in our microscope can be minimized to 0.1% by the BCOR and remain stable over longer microscope operation times. Images obtained from this microscope therefore normally require subsequent correction of neither linear magnification distortions nor coma by means of image processing, as is required for images obtained from standard electron microscopes.

¹Department of Structural Dynamics, MPI for Biophysical Chemistry, Göttingen, Germany. [✉]e-mail: hstark1@gwdg.de

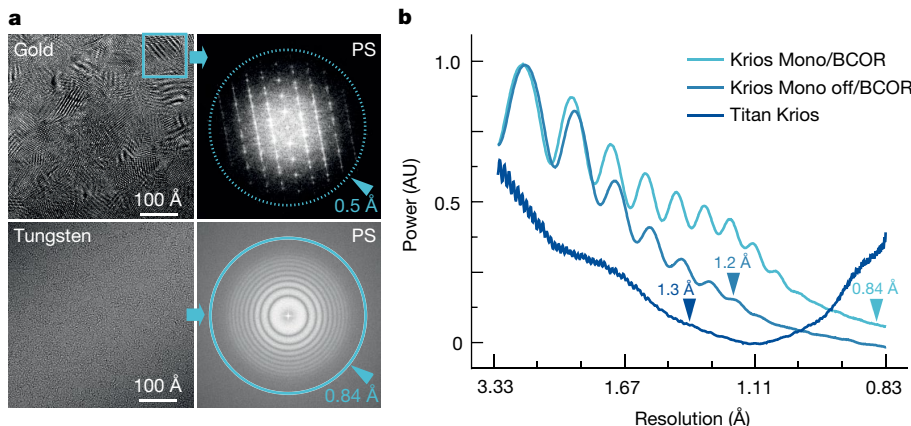


Fig. 1 | Optical performance of the Krios Mono/BCOR electron microscope.

a, High-resolution information transfer beyond 1 Å using a monochromator and BCOR corrector. Top, high-resolution image of a gold cross-grating specimen (left) showing reflections from a single crystal up to 0.5 Å in the Fourier transform (right; PS). Bottom, image of a tungsten specimen (left) and corresponding power spectrum (right; PS) showing information up to 0.84 Å according to equi-phase averaging as implemented in Gctf²². The power

spectra were cropped differently for better visualization. The performance of the microscope is perfectly reproducible after careful microscope alignment carried out before each data collection session. **b**, Performance of the Krios Mono/BCOR compared with the system without monochromator (Mono off) and a standard Titan Krios. Power spectra from tungsten obtained by equi-phase averaging. Arrowheads, maximum estimated resolution by Gctf.

Overall, the monochromated and aberration-corrected electron microscope (Titan Mono-BCOR) showed improved optical behaviour with diffraction spots up to 0.5 Å resolution in the computed power spectrum on a gold crystal (Fig. 1). This is an improvement in electron optical resolution of about 0.4 Å over a non-corrected- and non-monochromated Titan Krios electron microscope. Although the instrument clearly improves optical resolution, it is unclear how this translates into advances in the resolution attained for protein structures. Multiple factors impede the achievement of higher resolution in structures of biological specimens, the quality of the sample itself being the most dominant⁷. Biological molecules can be damaged during biochemical purification or the grid preparation process. In addition, a multitude of dynamic conformational states, a characteristic of macromolecular machines, are imaged. This often restricts the resolution that can be attained, as image classification methods sometimes fail to classify different conformational states accurately. Essentially, when attempting to achieve a higher resolution, the quality of both biological specimens and the electron microscope needs to be extraordinary.

Resolution and quality

Because of the beam sensitivity of biological objects⁸, they are imaged at a low electron dose and consequently the images suffer from a substantial amount of noise. To fight this, several hundred thousand or sometimes millions of particle images are averaged to calculate a single 3D structure by image processing⁹. The number of particle images that are needed to obtain a specific resolution can be described by an experimental *B*-factor¹⁰. The relationship between particle numbers and resolution becomes linear when the logarithm of the particle number is plotted against the reciprocal square of the resolution, and the experimental *B*-factor is determined from the slope of this curve (Fig. 2). The experimental *B*-factor represents a summary of all resolution-limiting factors of a given electron microscope and describes the overall quality of the instrumental setup. In addition, the *B*-factor plots enable us to extrapolate how many particles will be required to reach even higher resolution (Fig. 2b), assuming that exclusively image noise is crucial and no other resolution-limiting factors exist. This is, however, a best-case assumption, as additional hardware problems and aberrations are likely to occur when aiming for higher resolution.

Summarizing what we currently know from existing commercially available state-of-the-art electron microscope hardware and

its *B*-factors, we can predict that several hundred billion apoferitin particle images would be required to reach 1 Å resolution (Fig. 2). With the current speed of data acquisition this would translate into several hundred years of data recording and an unrealistic amount of computer power and data storage. These numbers clearly indicate that 1 Å-resolution reconstructions would be beyond any realistic expectations in cryo-EM considering the current commercially available best microscope hardware.

High-resolution structure of apoferitin

Structures of proteins in the 2–3.5 Å regime published so far show comparable features to those found using X-ray crystallography, even though the scattering of electrons and X-ray photons are substantially different physical events. However, this is expected to change in the very high-resolution regime. In X-ray crystallography, it is particularly challenging to see hydrogen atoms because of the limited photon scattering power of the single electron in a hydrogen atom¹¹. The situation in cryo-EM is different because electrons are scattered by the nuclear potential, which—in the case of H atoms—results in a larger scattering cross-section¹² compared to photons in X-ray crystallography¹³. Whereas H atoms become visible in X-ray maps typically only at resolutions close to 1 Å or better, they are expected to become visible at somewhat lower resolution in cryo-EM.

To obtain a high-resolution structure of apoferitin, we recorded images using gold-replaced Quantifoil grids mostly with a hole diameter of 1.2 μm, and 1.3 μm separation between holes, a pixel size corresponding to 0.492 Å and a total dose of about 50 electrons per Å², on a Falcon 3 detector in electron counting mode (Extended Data Fig. 2). The *B*-factor plot calculated from the initial data indicated that more than five million apoferitin particle images would be required to attain a resolution of 1.3 Å (a resolution at which hydrogen atoms might be visualized, owing to the differences in H-atom scattering cross-section between photons and electrons as discussed above). Optimization of grid preparation and imaging conditions allowed us to cross the 1.5 Å resolution barrier with only 22,000 particle images (*B*-factor of 36 Å²). Using a total number of about 1,000,000 particle images, we finally obtained a map at 1.25 Å resolution without applying any software correction for coma or higher-order aberrations. We corrected only for magnification changes that we observed over the time of data recording. Without magnification correction, the same data resulted

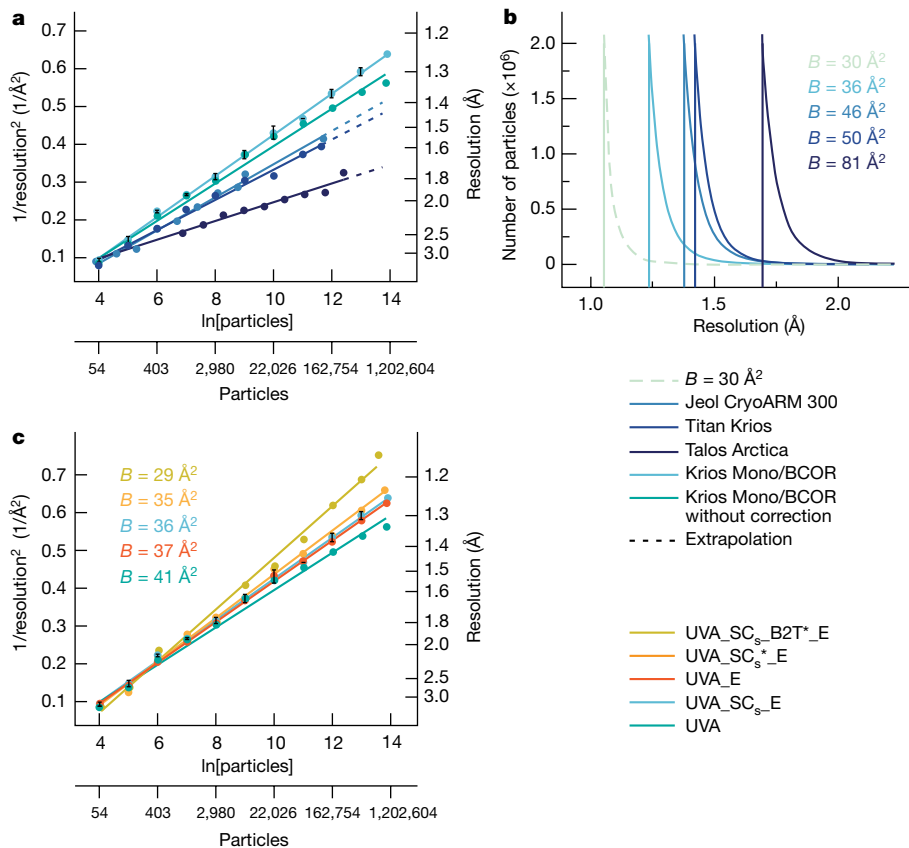


Fig. 2 | Performance comparison of cryo-EM systems. **a**, Performance as measured by the number of apoferritin particle images required to achieve a certain resolution cryo-EM structure. Remarkably, the Krios Mono/BCOR achieves superior performance without the need for in silico aberration correction. Krios Mono/BCOR with a B -factor of 36 \AA^2 (error bars were determined from three B -factor measurements. They are approximately the size of the data circles); Jeol CryoARM 300: EMPIAR-10248 and EMD-9865³; Titan Krios: re-computed from EMPIAR-10216; Talos Arctica: EMPIAR-10337 and EMDB-21024²³. **b**, Experimental B -factors result in hard resolution limits for a given cryo-EM imaging system. The explosive nature of the required particle numbers at high resolution becomes more readily apparent by displaying B -factors in a linear plot. Note the similar performance of the various microscope systems at resolutions up to 2 \AA . The B -factor of 36 \AA^2 obtained for the Krios Mono/BCOR indicates that it will become limiting for statistical particle number requirements only when attempting to attain structures slightly better than 1.25 \AA . A microscope that could break the 1 \AA resolution

barrier with acceptable particle number statistics needs to have a B -factor of 30 \AA^2 or better. **c**, B -factor dependence on various software corrections in Relion. Correcting only defocus and astigmatism (UVA) results in a B -factor of 41 \AA^2 and a map at 1.33 \AA resolution. This map behaves best in atomic model refinement. Additional Ewald sphere correction (E) improves the B -factor to 37 \AA^2 (map at 1.27 \AA resolution). The 1.25 \AA -resolution map was computed with additional micrograph scaling and spherical aberration (C_s) optimization (SC_s). The map with the nominally highest resolution of 1.15 \AA required additional software correction of higher order aberrations (B2T: coma and trifoil). Asterisk indicates that the correction was performed in image clusters depending on image or beam shift values. Even though the 1.15 \AA structure was nominally the best resolved map, it revealed some signs of overfitting. We consider the 1.25 \AA resolution structure ($B = 36 \text{ \AA}^2$) to be the best structure with acceptable behaviour during model refinement. Error bars were determined from three experiments with randomly selected particles for refinement. For further information, see Extended Data Table 1.

in a map at 1.33 \AA resolution. The sharpened 1.25 \AA map—in contrast to X-ray maps at this resolution—shows well-defined additional densities that agree with the positions of hydrogens on almost all atoms (Fig. 3, Extended Data Figs. 3, 4, Supplementary Video 1), when using low thresholds for map visualization. At higher thresholds, almost completely separated densities for individual C, O and N atoms are visible in most areas of the map (Fig. 3, Supplementary Video 1). Furthermore, the resolution of the map is sufficient to observe a sulfur chemical modification in apoferritin (Extended Data Fig. 5), which to the best of our knowledge has not been visualized as yet.

Resolution versus map quality

How do the various cryo-EM structures for apoferritin compare both in terms of required particle statistics and map quality? In cryo-EM, the resolution of the map is estimated by the correlation of two independently calculated structures in various resolution shells in Fourier space, termed the Fourier shell correlation¹⁴ (FSC). The FSC provides

a single number for the estimated resolution, but this number is not entirely independent from data processing procedures¹⁵. As the FSC is not a good reporter for the quality of the calculated density map, we were aiming for another map quality comparison. In principle, the degree to which the map can be interpreted in atomic modelling, particularly with respect to the bound solvent and subsequent refinement of the model, represents such a measure. Atomic model refinement at intermediate resolutions rely strongly on prior knowledge of (protein) chemistry, such as bond lengths, geometry and additional constraints such as the planarity of aromatic systems. At atomic resolution, the density of information gleaned from the structure should allow atomic modelling independent of constraints and enable the experimental observation of slight deviations from standard chemistry. Such deviations frequently arise and are essential for understanding how proteins catalyse seemingly impossible reactions. Sub-ångström-resolution crystallography reveals such distortions, which enhance the enzyme reactivity of enzymatic intermediates^{2,16}. In addition, such detailed, experimental and unbiased views of protein architecture can provide

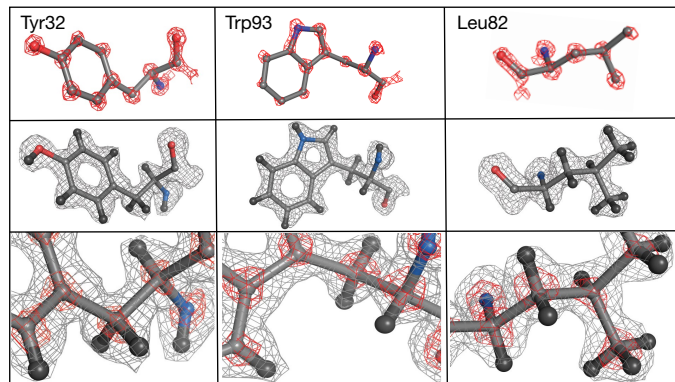


Fig. 3 | True atomic resolution. Visualization of individual atoms and hydrogens at 1.25 Å resolution. Three apoferritin residues are shown at high (red mesh) and low (grey mesh) density thresholds. The true atomic resolution of our map is shown in the first row by the clear separation of individual C, N and O atoms at high thresholds. The second row shows density that agrees with hydrogen atom positions in all parts of the individual amino acid side chains. A ball and stick representation for the hydrogen atoms (black) is included in the atomic model. Similar visibility of density for hydrogen atoms requires about 1 Å or better resolution in X-ray crystallographic structures (Extended Data Fig. 3). The third row shows close-up views of the three amino acids using both density thresholds simultaneously.

invaluable insights into binding pockets for the design of specific drugs^{17,18}. In the case of cryo-EM density maps, features that deviate from perfect geometry can either reflect true changes or be caused by image processing errors and/or optical aberrations. Whereas a certain deviation from perfect geometry is allowed, a good-quality high-resolution cryo-EM map should allow the modelling of proteins with no overall systematic deviations from normal chemical structure and allow the refinement of atomic models against the experimental map in an unconstrained fashion. Other quality estimators are the abundance of ordered solvent, which can be modelled at a given resolution, and the coordination distances of ordered solvent molecules from the protein.

To assess map quality, independent of resolution differences, we compared a 1.55 Å-resolution structure from a random subset of the data acquired in our instrument, with the highest-resolution apoferritin structure at 1.54 Å (Extended Data Fig. 6). Notably, to achieve this resolution in our microscope, only about 22,000 particle images were required; this number can be recorded in less than 2 h with the current speed of data collection of our microscope (100 videos per hour, Extended Data Fig. 7). This is roughly 5.5 times fewer particles than those required to achieve the 1.54 Å structure using the Jeol microscope³. Even though the nominal resolution is comparable, we were able to reliably model 1,750 more water molecules in our unsharpened map, applying the same modelling procedures (Extended Data Fig. 6). This significant difference can be attributed to the improved optical quality of the Titan Mono-BCOR microscope. Whereas no beam-tilt-induced coma is present in our data and no beam-tilt software correction was applied to calculate our map, a substantial amount of beam tilt was present in the data recorded in the Jeol CryoARM microscope because of some instabilities of the cold field emitter after flashing. The latest developments in the Relion software^{19,20} allow the a posteriori computational correction of beam-tilt induced coma and even higher-order aberrations. However, neither the accuracy nor the validity of applying these corrections has been evaluated quantitatively.

By applying higher-order aberration correction in Relion 3.1 to the full dataset, we were able to improve the nominal resolution to 1.15 Å. However, after model building and refinement we refrained from using the 1.15 Å-resolution map for further analysis because of quality issues

observed in the refined model. The 1.15 Å structure revealed no data in the highest-resolution shells and no additional structural detail that would support the model, illustrating that reported FSC-based resolution claims can potentially be affected by image processing. One possible explanation for the discrepancy between nominal and true resolution might be that some optical aberrations, such as coma, potentially lead to systematic errors that cannot be detected by the FSC and may result in overestimation of resolution²¹. The map at 1.33 Å resolution, for which no corrections other than those for defocus and for astigmatism were performed, behaved best during model refinement. It also provided the best crystallographic *R* values and the best bond geometries (Extended Data Table 1).

Expected improvements with new EM hardware

For samples with perfect biochemical quality and stability, the resolution and quality of the 3D density map depend on the electron microscope hardware; we have shown here that atomic resolution can be attained. For the vast majority of macromolecular complexes, improvements in resolution will also depend strongly on improvements in biochemical sample quality and on image classification tools that can handle continuous conformational motion in the data. Even though it is possible to obtain 1.5 Å resolution with only 22,000 particles, the required particle numbers can be several orders of magnitudes higher for non-symmetric and more dynamic complexes. For asymmetric particles with ten conformational states that need to be computationally sorted, the acquisition of an unrealistic number (more than five million) of particles would be required using the Titan Mono-BCOR microscope. Further improvements in image recording speed by faster cameras and optimized data acquisition schemes will contribute substantially to the achievement of such goals in the future. Realistically, high-throughput cryo-EM structure determination at resolutions that allow the visualization of individual atoms and hydrogens is not likely to be possible in the near future. However, if resolutions in the 1.5–2 Å range are sufficient, a microscope such as that presented here can be powerful enough to determine even several structures a day for a biochemically well-behaved and symmetric macromolecular complex. At slightly lower resolution aims, the microscope itself becomes an increasingly non-decisive factor and in the 3–3.5 Å-resolution range, any currently available microscope with a direct electron detector can be used because the required particle numbers can be recorded within a reasonable time (Fig. 2a). At very high resolution, each electron microscope does have strict limits in its capabilities because of the exponential nature of the required particle numbers once the optical limits of the respective system are reached (Fig. 2b, c). Our current microscope has an experimental *B*-factor of 36 Å² (without software-based aberration correction), which makes it almost impossible to obtain a resolution better than 1.2 Å even for a perfect sample. Further improvements in electron microscope hardware are therefore essential if we are to get closer to, or eventually break, the 1 Å resolution barrier. This work represents a substantial step forward in this direction, as it provides the structure of apoferritin at an extremely high resolution that allows its atomic details to be investigated.

To reach true atomic resolution on a more regular basis for more challenging complexes will also require improvements in grid preparation, image classification software and microscope hardware. These improvements in all aspects of cryo-EM technologies can be expected to become available within the near future. For instance, next-generation electron microscopes, detectors and energy filters have the potential to make a substantial contribution to further improved microscope performance, reaching *B*-factors that would allow atomic-resolution structure determination (*B* < 30 Å²) with lower demands on particle statistics. This would enable structures to be determined at atomic resolution more frequently for many more macromolecular complexes, improving our understanding of the catalytic mechanisms of proteins

and aiding in the development of new drugs based on high-resolution, high-quality 3D structures of proteins.

Online content

Any methods, additional references, Nature Research reporting summaries, source data, extended data, supplementary information, acknowledgements, peer review information; details of author contributions and competing interests; and statements of data and code availability are available at <https://doi.org/10.1038/s41586-020-2833-4>.

1. Kühlbrandt, W. The resolution revolution. *Science* **343**, 1443–1444 (2014).
2. Lüdtke, S. et al. Sub-Ångström-resolution crystallography reveals physical distortions that enhance reactivity of a covalent enzymatic intermediate. *Nat. Chem.* **5**, 762–767 (2013).
3. Kato, T. et al. The 1.54 Å resolution structure of apoferritin by CRYOARM300 with Cold-FEG. *Microsc. Microanal.* **25**, 998–999 (2019).
4. Hamaguchi, T. et al. A new cryo-EM system for single particle analysis. *J. Struct. Biol.* **207**, 40–48 (2019).
5. Tiemeijer, P. C., Bischoff, M., Freitag, B. & Kisielowski, C. Using a monochromator to improve the resolution in TEM to below 0.5 Å. Part I: Creating highly coherent monochromated illumination. *Ultramicroscopy* **114**, 72–81 (2012).
6. Müller, H. et al. Aplanatic imaging systems for the transmission electron microscope. *Nucl. Instrum. Meth. A* **645**, 20–27 (2011).
7. Stark, H. & Chari, A. Sample preparation of biological macromolecular assemblies for the determination of high-resolution structures by cryo-electron microscopy. *Microscopy (Oxf.)* **65**, 23–34 (2016).
8. Karuppasamy, M., Karimi Nejadash, F., Vulovic, M., Koster, A. J. & Ravelli, R. B. Radiation damage in single-particle cryo-electron microscopy: effects of dose and dose rate. *J. Synchrotron Radiat.* **18**, 398–412 (2011).
9. Frank, J. Generalized single-particle cryo-EM—a historical perspective. *Microscopy (Oxf.)* **65**, 3–8 (2016).
10. Rosenthal, P. B. & Henderson, R. Optimal determination of particle orientation, absolute hand, and contrast loss in single-particle electron cryomicroscopy. *J. Mol. Biol.* **333**, 721–745 (2003).
11. Bracewell, B. L. & Veigle, W. J. in *Advances in X-Ray Analysis* Vol. 15 (eds Heinrich, K. F. J. et al.) 352–364 (Springer US, 1972).
12. Williams, J. F. Electron scattering from atomic hydrogen. III. Absolute differential cross sections for elastic scattering of electrons of energies from 20 to 680 eV. *J. Phys. B* **8**, 2191–2199 (1975).
13. Carter, C., March, N. H. & Vincent, D. X-ray and electron scattering by molecular hydrogen. *Proc. Phys. Soc.* **71**, 2–16 (1958).
14. Harauz, G. & van Heel, M. Exact filters for general geometry three dimensional reconstruction. *Optik (Stuttg.)* **73**, 146–156 (1986).
15. Grigorieff, N. Resolution measurement in structures derived from single particles. *Acta Crystallogr. D* **56**, 1270–1277 (2000).
16. Heinrich, D., Diederichsen, U. & Rudolph, M. G. Lys314 is a nucleophile in non-classical reactions of orotidine-5'-monophosphate decarboxylase. *Chemistry* **15**, 6619–6625 (2009).
17. Homans, S. W. Water, water everywhere—except where it matters? *Drug Discov. Today* **12**, 534–539 (2007).
18. Schiebel, J. et al. Intriguing role of water in protein-ligand binding studied by neutron crystallography on trypsin complexes. *Nat. Commun.* **9**, 3559 (2018).
19. Zivanov, J. et al. New tools for automated high-resolution cryo-EM structure determination in RELION-3. *eLife* **7**, e42166 (2018).
20. Zivanov, J., Nakane, T. & Scheres, S. H. W. Estimation of high-order aberrations and anisotropic magnification from cryo-EM data sets in RELION-3.1. *IUCrJ* **7**, 253–267 (2020).
21. Bromberg, R., Guo, Y., Borek, D. & Otwinowski, Z. High-resolution cryo-EM reconstructions in the presence of substantial aberrations. *IUCrJ* **7**, 445–452 (2020).
22. Zhang, K. Gctf: Real-time CTF determination and correction. *J. Struct. Biol.* **193**, 1–12 (2016).
23. Wu, M., Lander, G. C. & Herzik, M. A., Jr. Sub-2 Angstrom resolution structure determination using single-particle cryo-EM at 200 keV. *J. Struct. Biol. X* **4**, 100020 (2020).

Publisher's note Springer Nature remains neutral with regard to jurisdictional claims in published maps and institutional affiliations.

© The Author(s), under exclusive licence to Springer Nature Limited 2020

Methods

Apoferitin expression and purification

A cDNA encoding the K86Q variant of the human ferritin heavy chain with codons optimized for expression in *Escherichia coli* was obtained from Geneart (Regensburg) and subcloned as a NdeI–XhoI fragment into the pRSET-A expression plasmid. The untagged protein was obtained by transformation of this plasmid into BL21(DE3). Expression was performed in Terrific Broth medium containing ampicillin (100 µg/ml) and glucose (1% w/v), cells were induced at OD₆₀₀ = 0.8 with 1 mM isopropyl β-D-1-thiogalactopyranoside (IPTG) for 3.5 h at 37 °C and the harvested cells were then stored at -20 °C. To purify the protein, the cell pellet was resuspended in 15 mM Tris-HCl (pH 7.4), 150 mM NaCl, 10 mM DTT, 10 mM benzamidine-HCl, 10 mM EDTA, 1 mM PMSF, 2.5% (w/v) sucrose, and lysed by the addition of 1% Triton X-100 and passage through a high-pressure disruptor (Emulsiflex). A cleared lysate was prepared by centrifugation at 30,000g, followed by the precipitation of nucleic acids by the addition of 3% (w/v) streptomycin sulfate and centrifugation at 20,000g. The supernatant was incubated at 75 °C for 20 min to precipitate *E. coli* proteins, followed by centrifugation at 20,000g for 30 min. The resulting supernatant was then subjected to ammonium sulfate fractionation by the addition of powder to a saturation of 60% (w/v). The resulting pellet was resuspended in 15 mM Tris-HCl (pH 7.4), 150 mM NaCl, 10 mM DTT and 0.1% (w/v) LMNG and subjected to density gradient centrifugation on 10–40% (w/v) sucrose gradients in a Surespin CA 630-36 rotor at 25,000 rpm, 18 °C for 19 h. Fractions containing ferritin were identified by SDS-PAGE, pooled and subjected to dialysis against 50 mM MES, 150 mM NaCl, 0.5% thioglycolic acid (pH 6.5) for 24 h, followed by dialysis against 15 mM Tris-HCl (pH 7.4), 150 mM NaCl and 2.5% (w/v) sucrose for 24 h at room temperature. The resulting apoferitin was then precipitated by the addition of ammonium sulfate to 60% saturation and the pellet resuspended with 15 mM Tris-HCl (pH 7.4), 150 mM NaCl, 1 mM EDTA and 0.01% (w/v) LMNG. The sample was then subjected to density gradient centrifugation on 10–40% (w/v) sucrose gradients in a SW40Ti rotor at 30,000 rpm at 18 °C for 16 h. Fractions containing ferritin were identified by SDS-PAGE, pooled and buffer exchanged to 1× PBS by concentration in an Amicon spin concentrator and frozen in liquid nitrogen and stored in small aliquots at a concentration of 10 mg/ml.

Cryo-EM grid preparation

For alignment purposes, UltrAuFoil R1.2/1.3 and R1.5/1.0 300-mesh grids (Quantifoil, Jena, DE) were pre-floated with custom-made continuous carbon foil covering ~25% of the grid area. Grids were glow discharged for 10 s with a glow discharger built in-house under low vacuum shortly before sample application. 4 µL of purified apoferitin (~3.5 mg ml⁻¹) was applied to glow-discharged grids, which were blotted and plunge-frozen with a Vitrobot Mark IV (Thermo Fisher Scientific) operated at 4 °C and 100% humidity; the blotting time was set to be 6.5 s and 7.5 s for UltrAuFoil R1.2/1.3 and R1.5/1.0 grids, respectively.

Cryo-EM data acquisition and image processing

All cryo-EM data were collected in nanoProbe mode on a Titan Krios electron microscope operating at 300 kV equipped with a monochromator (Thermo Fisher Scientific) and an aplanatic image corrector (BCOR; CEOS). The monochromator was tuned to operate at 3 kV potential and excitation (0.8) to obtain an energy spread of the source of about 0.1–0.15 eV. The monochromator reveals a certain amount of thermal drift that was corrected for by the monochromator shift coils during automated data collection whenever the camera counts went below a certain threshold. The automated re-centring of the monochromator has no impact on other alignments. The BCOR was set-up to correct for off-axial aberrations, beam/image shift induced coma and for linear magnification distortions. For each cryo-EM dataset, the BCOR was tuned with the signals from the amorphous carbon (i) to

correct the phase errors introduced by on-axis electron optical aberrations to less than 45° at scattering angles ≥17 mrad, which is equivalent to ≤1.16 Å resolution; and (ii) to reduce linear distortions to ≤0.2%. These alignments are at least stable for an entire day and are checked on a daily basis for longer data acquisitions. The daily fine tuning of the entire microscope alignment takes about 15 min.

We collected 10,398 videos with 40 fractions each. The exposure time was over 18.54 s with a dose of ~1.25 e⁻/Å² per fraction in electron counting mode using a Falcon III direct electron detector (Thermo Fisher Scientific) at a nominal magnification of 120,000× (~0.492 Å per pixel) and 0.3–1 µm underfocus resulting in a total dose of ~50 e⁻/Å². An adapted version of the software EPU (v2.4.0.78 Patch-2882REL4, Thermo Fisher Scientific) was used to acquire data by beam/image shift over up to 3 × 3 holes; for R1.2/1.3 grids, three movies were acquired per hole, and for R1.5/1.0 grids, five movies per hole. The data were acquired over 40 acquisition sessions resulting in 40 datasets, which were each pre-processed independently.

All image processing was performed using RELION 3.1²⁰ unless indicated otherwise. Global motion correction and dose-weighting were performed with a *B*-factor of 150 and the dose-weighted micrographs were used for CTF estimation by Gctf 1.06²². Particles were picked with reference to 2D templates and extracted with 2 × 2 binning (0.984 Å per pixel, 180 × 180 pixel box). Two rounds of reference-free 2D classifications were performed to remove bad particles. The remaining good particles were re-centred, and re-extracted in full size in a 480 × 480 pixel box (0.492 Å per pixel) and subjected to 3D refinement; all 3D procedures were performed imposing octahedral symmetry. The structure of mouse apoferitin (EMDB-9599, REF) was low-pass filtered to 20 Å and used as a reference for initial 3D refinements. A first round of CTF refinement was performed on the refined particles to correct for per-micrograph defocus and per-micrograph astigmatism. Then, particle motion and the corresponding per-frame relative *B*-factors were estimated by Bayesian polishing and the polished particles were subjected to a second round of 3D refinement. Another round of CTF refinement was performed to correct for per-particle defocus and per-particle astigmatism. Afterwards, the particles were again subjected to Bayesian polishing and a third round of 3D refinement. The procedure was repeated for all 40 datasets independently.

Particles from individual datasets were defined as a unique optics group each, and all 1,466,774 particles were combined for all further image processing. CTF refinements were performed to correct first for magnification anisotropy, then for fourth-order aberrations (to refine the spherical aberration constants, which varied slightly owing to the BCOR tuning) and, finally, for per-particle defocus, per-particle astigmatism, followed by another 3D refinement. Ewald sphere correction²⁴ was performed on the two resulting half-maps, yielding a final reconstruction with a resolution of 1.27 Å for a pixel size of 0.492 Å, as calibrated by atomic-model refinement (see below). Subsequently, particle images were re-polished on the basis of the new 3D structure and windowed and refined in a 600 × 600 pixel box to account for the high-resolution information spread introduced by defocus. The refined particles were reduced to 1,090,676 particle images, excluding particles with a defocus of >9,000 Å and a maximum-value-probability distribution of <0.04. From the reduced dataset, half-maps were reconstructed using Ewald sphere correction²⁴ resulting in a 3D reconstruction at a final resolution of 1.25 Å (Extended Data Fig. 2b). Applying higher-order aberration correction in Relion improved the nominal resolution to 1.15 Å. However, we did not use this map for further analysis because of the discrepancy between FSC-based and true resolution and the quality issues that became apparent during atomic model refinement.

B-factor plots

For the *B*-factor plot (Fig. 2a), the total set of 1,090,676 particle images from the final refinement was randomly resampled into smaller

subsets, half-maps were reconstructed for each subset using Ewald sphere correction and FSCs were computed by cropping the half-maps to 480×480 pixel boxes for subsets with ≥ 148 particles or 420×420 pixel boxes for subsets with 55 particles. For the standard Titan Krios, we re-evaluated data from EMPIAR-10216 mainly as described (<https://twitter.com/radodanev/status/1022265459666694144?lang=en>) but with modifications to at least partially account for off-axial aberrations by splitting the micrographs into nine subsets²⁰. This procedure slightly improved the final resolution from the stated 1.62 Å to 1.59 Å.

Atomic model building and refinement

Atomic model building and refinement are highly dependent on the achieved map resolution. Model refinements in the 2–3.5 Å-resolution regime require a substantial amount of weight from prior information about protein chemistry because the maps themselves do not show enough structural details. Using prior chemical information avoids the generation of atomic models that agree well with the data but would violate prior chemical knowledge. At true atomic resolution, the calculated density map is supposed to be detailed enough to position individual atoms and models can be refined without using prior information about chemical bonds. Atomic-resolution structure determination is therefore essential to understand chemical reaction mechanisms because it is the slight deviation from normal chemistry that drives chemical reactions. Normally, cryo-EM maps require a certain amount of sharpening to visualize all the high-resolution structural details but it turned out that normal map sharpening procedures are not compatible with crystallographic model refinements. Thus, only unsharpened maps were used for the refinement of models, as the utilization of sharpened maps resulted in substantial distortions of model geometry. An initial model was generated using the deposited K69Q human ferritin heavy chain model (2CEI). The 24-mer for model refinement was assembled using MOLREP (11.7.02)²⁵ anew into every experimental EM map using the 2CEI monomer stripped of all solvent. After rigid body refinement and positional refinement in Refmac5 (5.8.0258)²⁶ essentially as described²⁷, the model was adjusted to the density manually in Coot (0.8.9.2)²⁸. After an additional round of positional refinement in Refmac5, solvent molecules were added interactively in Coot, followed by an additional round of refinement in Refmac5.

Reporting summary

Further information on research design is available in the Nature Research Reporting Summary linked to this paper.

Data availability

The atomic models have been deposited in the Protein Data Bank (PDB) with the following accession codes: 1.56 Å structure (COW) 6Z9F, 1.55 Å structure 6Z9E, 1.33 Å structure 7A6B, 1.25 Å structure 6Z6U, and 1.15 Å structure 7A6A. The cryo-EM maps have been deposited in the Electron Microscopy Data Bank as follows: 1.56 Å map (COW, EMD-11122), 1.55 Å map (EMD-11121), 1.33 Å map (EMD-11669), 1.25 Å map (EMD-11103) and 1.15 Å map (EMD-11668).

24. Russo, C. J. & Henderson, R. Ewald sphere correction using a single side-band image processing algorithm. *Ultramicroscopy* **187**, 26–33 (2018).
25. Vagin, A. & Teplyakov, A. Molecular replacement with MOLREP. *Acta Crystallogr. D* **66**, 22–25 (2010).
26. Murshudov, G. N. et al. REFMAC5 for the refinement of macromolecular crystal structures. *Acta Crystallogr. D* **67**, 355–367 (2011).
27. Singh, K. et al. Discovery of a regulatory subunit of the yeast fatty acid synthase. *Cell* **180**, 1130–1143.e1120 (2020).
28. Emsley, P. & Cowtan, K. Coot: model-building tools for molecular graphics. *Acta Crystallogr. D* **60**, 2126–2132 (2004).

Acknowledgements We thank J. E. Schliep for his contribution in the early phase of the project; M. Lütich for setting up the computational facilities; and M. Link and S. Dalaikhur for their technical contribution in the initial setup of the microscope. This work was supported by the Max Planck Society and the Deutsche Forschungsgemeinschaft (grants SFB 860 to H.S.).

Author contributions H.S., K.M.Y. and N.F. set up the Krios Mono/BCOR microscope. E.P. and A.C. developed the purification strategy and E.P. purified the complex. K.M.Y. prepared grids and collected EM data. K.M.Y. and N.F. did the cryo-EM image processing analysis. A.C. built and refined the atomic models. The manuscript was written by H.S. with input from all authors. H.S. initiated and orchestrated the project.

Competing interests The authors declare no competing interests.

Additional information

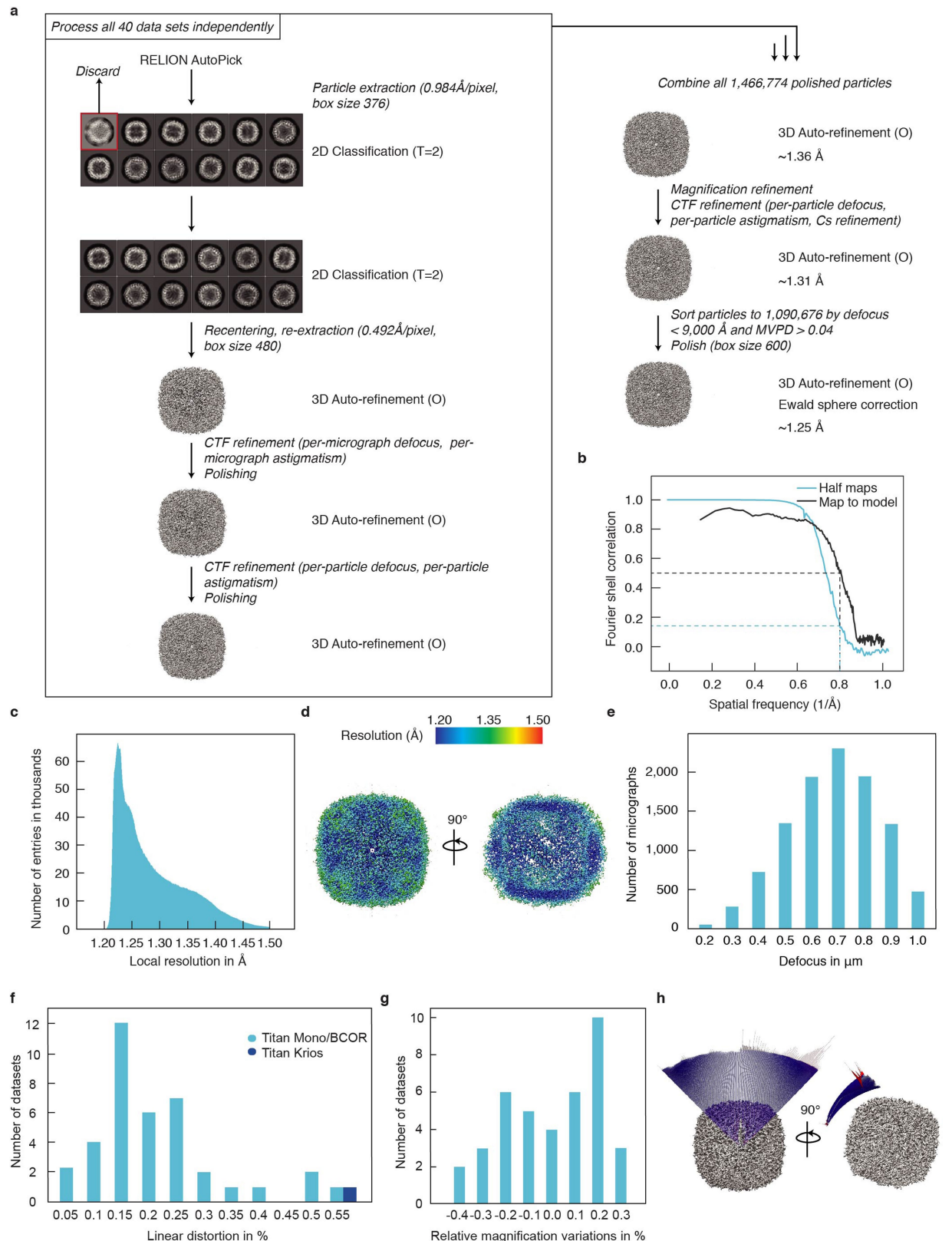
Supplementary information is available for this paper at <https://doi.org/10.1038/s41586-020-2833-4>.

Correspondence and requests for materials should be addressed to H.S.

Peer review information *Nature* thanks Henning Stahlberg, Serban Ilca and the other, anonymous, reviewer(s) for their contribution to the peer review of this work.

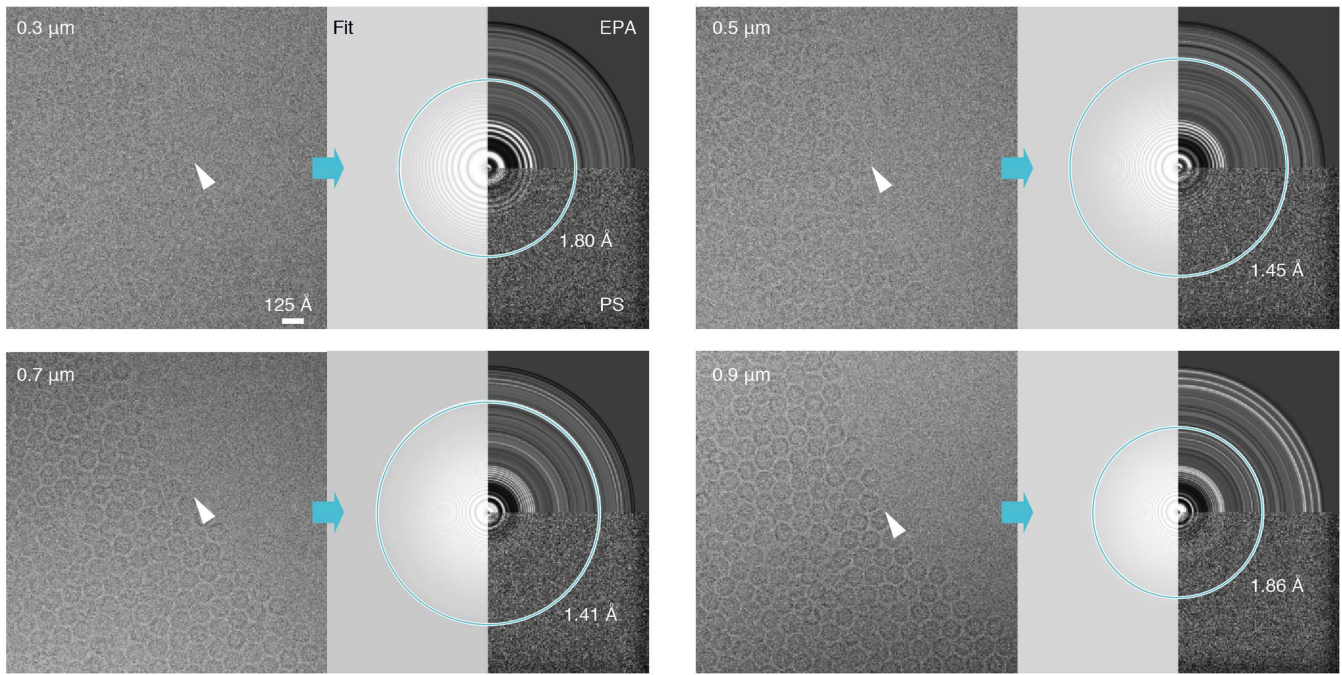
Reprints and permissions information is available at <http://www.nature.com/reprints>.

Article



Extended Data Fig. 1 | Cryo-EM structure determination. **a**, Image processing pipeline. See Methods for details. **b**, Fourier-shell-correlation plots for independently refined half-maps (Half maps) and full map versus model (Map to model). **c**, Histogram of local resolution for the final 1.25 Å map obtained with relion postprocess using a small soft spherical mask. **d**, Final map colored by local resolution. **e**, Defocus distribution for the total set of

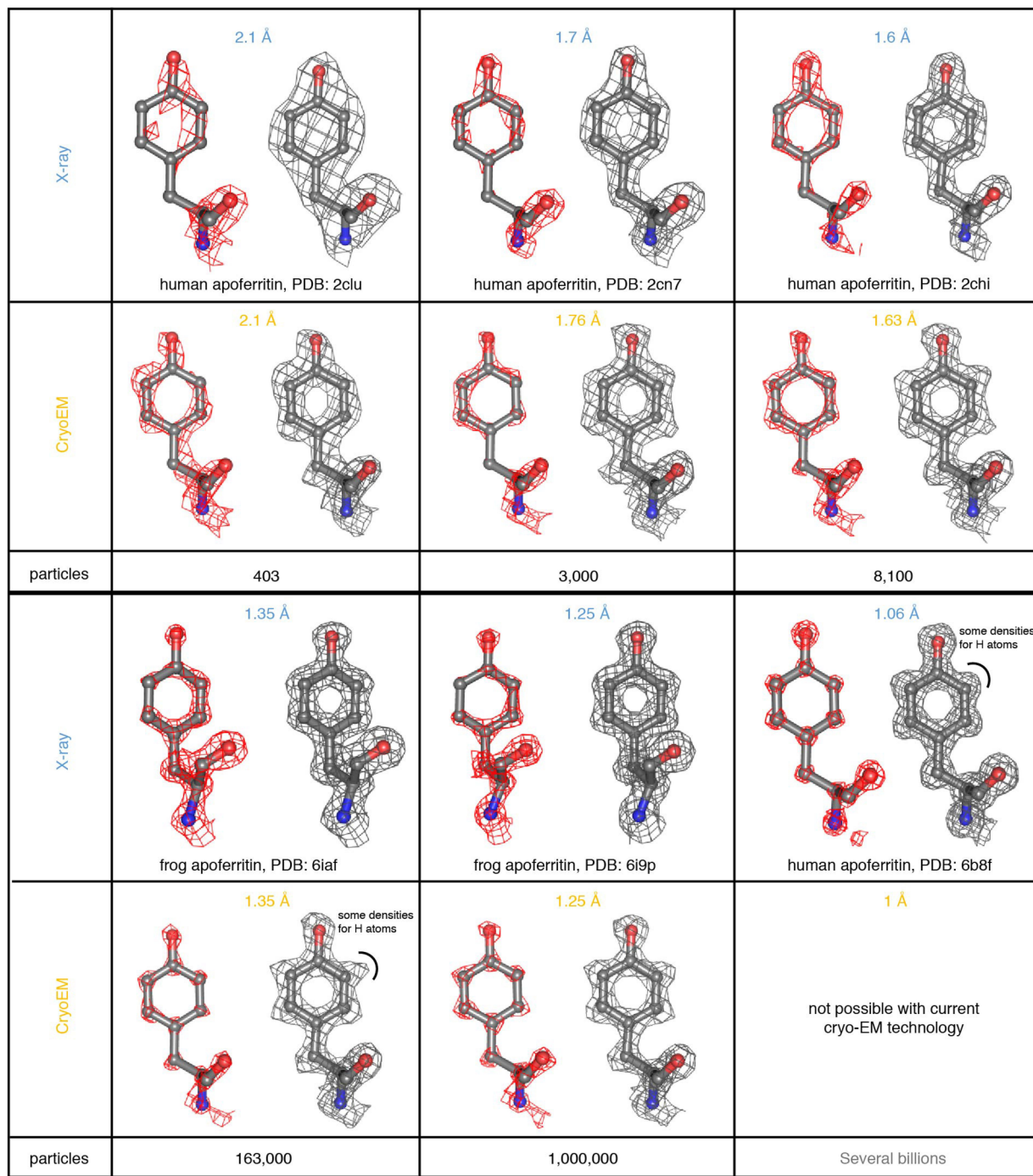
10,398 micrographs. **f**, Linear magnification distortions as estimated by `relion_ctf_refine` for the present Krios Mono/BCOR data and data from a standard Titan Krios (EMPIAR-10216). **g**, Relative magnification variation in the present data as determined by `relion_ctf_refine`. **h**, Angular distribution for the final map.



Extended Data Fig. 2 | Low-dose cryo-EM micrographs of human apo ferritin. Exemplary micrographs (left) acquired with a total dose of $\sim 50\text{e}\text{-}\text{\AA}^2$ are shown with their power spectra (PS), equi-phase average (EPA) and the fit of the contrast transfer function (Fit). A total number of 10.398 similar micrographs has been recorded. Numbers indicate the respective defocus in

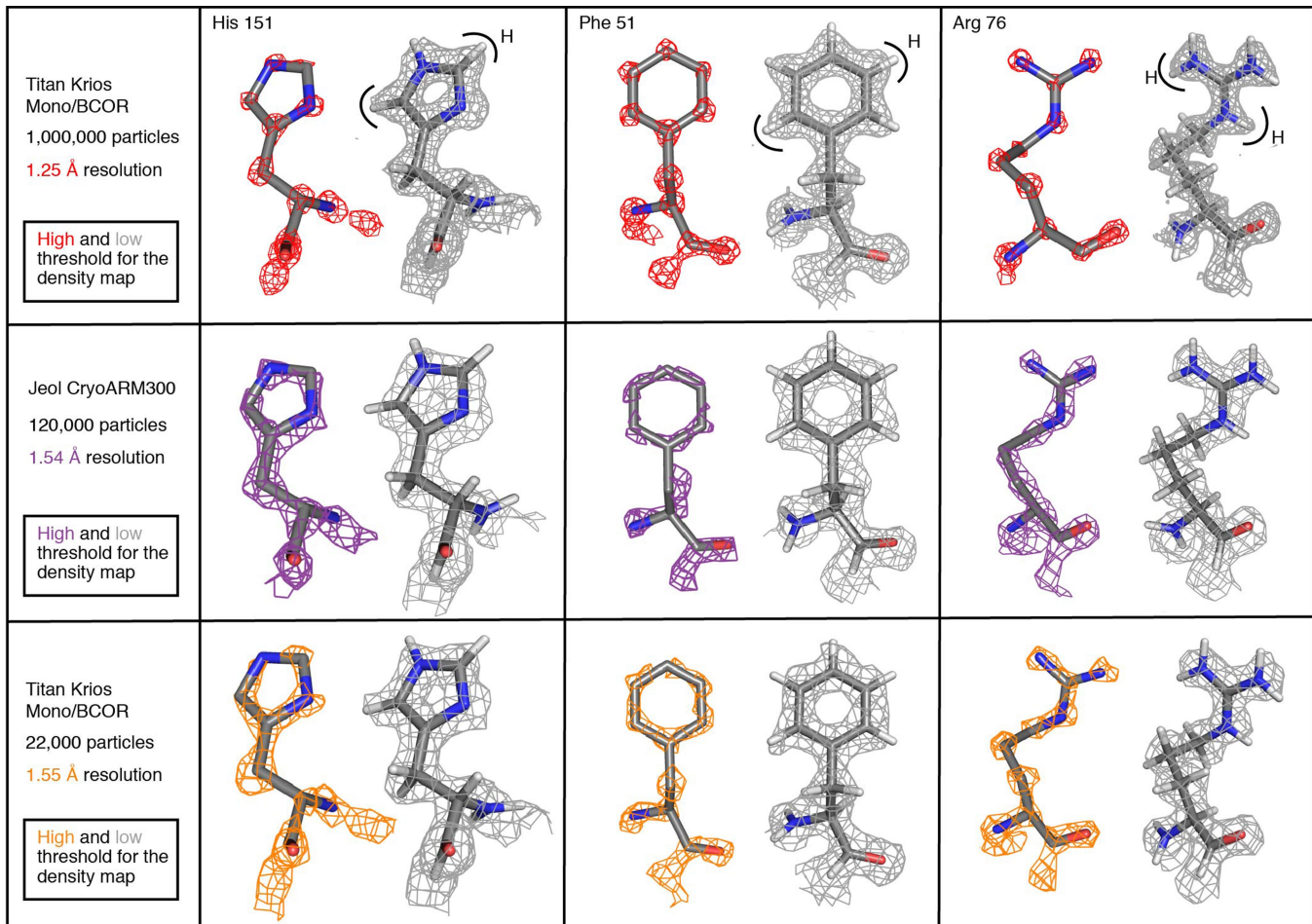
μm and the maximum resolution (in \AA) in the power spectra as estimated by Gctf²². White arrow heads denote the transition from areas with particles in dense packing to areas devoid of particles indicating a very thin layer of vitrified ice, as required for high-resolution imaging.

Article



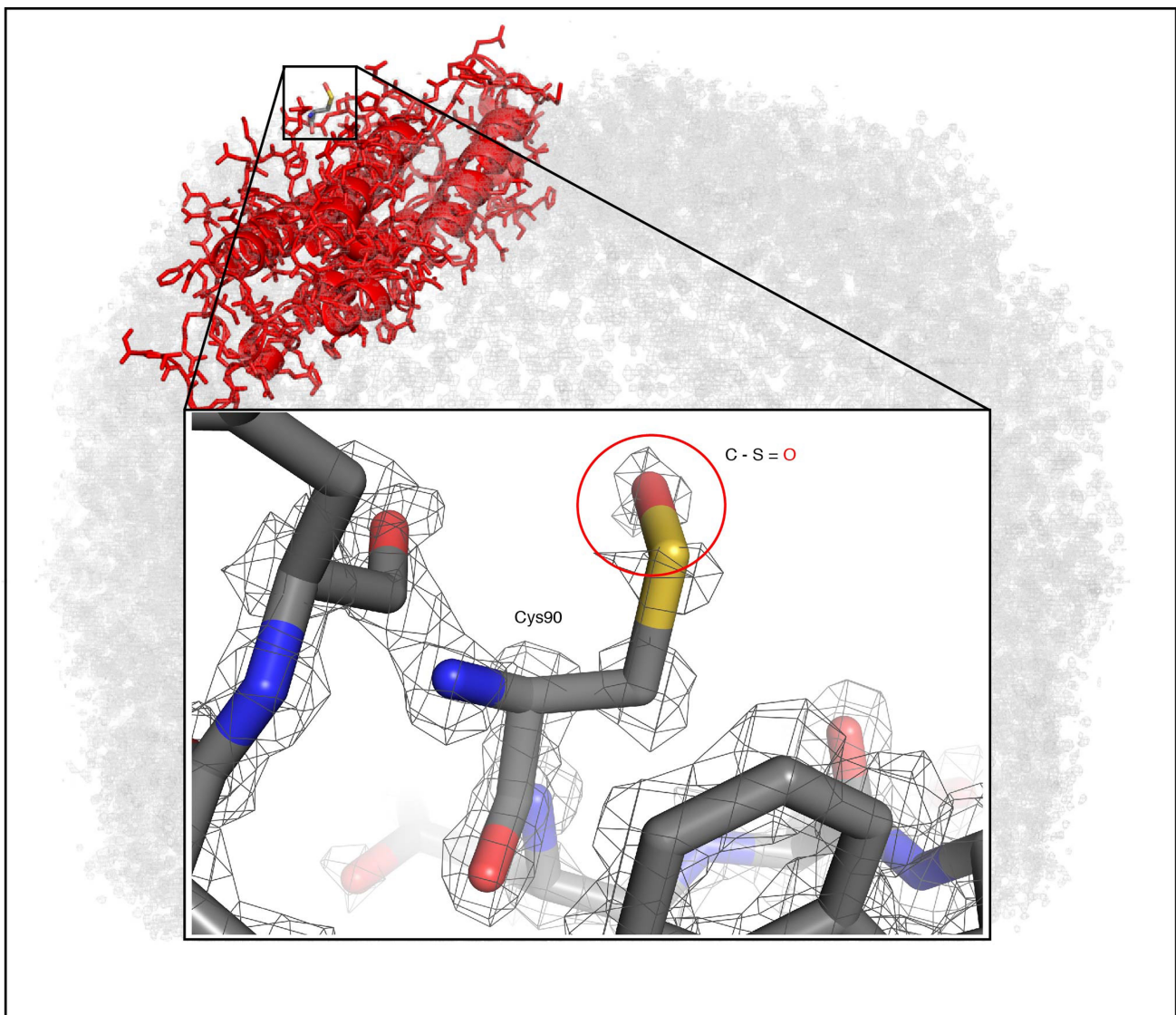
Extended Data Fig. 3 | Comparing high-resolution features obtained by X-ray crystallography and cryo-EM. For the comparison, we selected the same tyrosine residue (Tyr32 in human apoferitin, Tyr34 in frog) from our structures obtained at different resolutions with published crystallographic data of apoferritin at the indicated resolution. The same residue is shown at high (red) and low (grey) threshold to better judge the structural details and the map quality. Density that can be attributed to hydrogen atoms can barely be seen in any of the X-ray structures. Even at 1.06 Å resolution only weak

density for hydrogens can be detected while the cryo-EM reconstruction already reveals some density for hydrogens at 1.35 Å resolution. At high thresholds, the separation into clearly distinct atoms can only be seen in the 1.06 Å resolution X-ray map but not in lower resolution X-ray data. In case of our cryo-EM reconstructions we can see individual atoms starting at 1.35 Å resolution or better. Cryo-EM structures at 1 Å resolution are currently not possible because they would require unrealistically high particle number statistics even with the Krios Mono/BCOR microscope (see Fig. 2).



Extended Data Fig. 4 | Structural features of our cryo-EM maps at 1.55/1.25 Å resolution compared to the thus far reported highest-resolution map at 1.54 Å resolution (EMDB-9865). Three apoferritin residues (His151, Phe51, Arg76) are shown at two different density thresholds in three cryo-EM maps. Row one depicts our present high-resolution map at 1.25 Å; resolution and row three shows a structure at 1.55 Å; resolution obtained from a smaller subset of the same data. Only 22,000 particles were necessary for this reconstruction to obtain 1.55 Å resolution which is a 5.5× lower particle statistics compared to the

1.54 Å Jeol CryoARM300 map (second row). The low-threshold density meshes are always shown in grey and H atoms (white sticks) are included in the corresponding atomic models. Only in the Krios Mono/BCOR structure at 1.25 Å; resolution density becomes visible to accommodate all hydrogen atoms. At higher thresholds the two structures at 1.54 Å and 1.55 Å resolution nicely maintain the shapes of the sidechains but only in the structure at 1.25 Å; resolution individual atoms become clearly separated from each other indicating true atomic resolution.

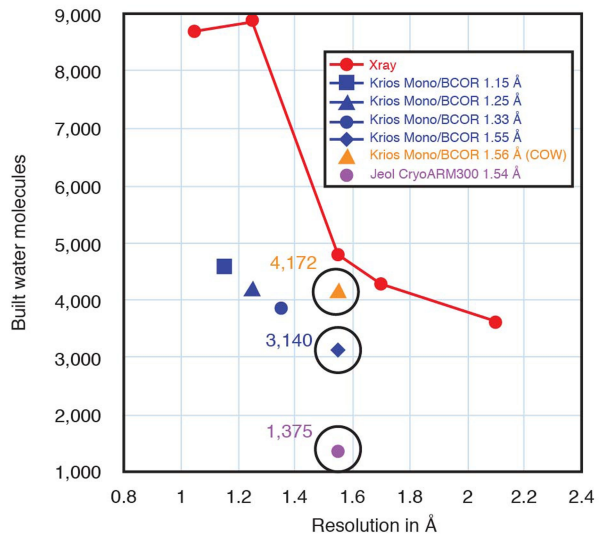


Extended Data Fig. 5 | Visualization of a single atom chemical modification. Cysteine 90 of human apo ferritin is located at the surface of the macromolecular complex. The solvent-exposed regions are usually determined at lower local-resolution in cryo-EM but in our high-resolution

structure it is still sufficient to visualize a single atom oxygen modification (marked by a square on the entire molecule and by the red circle in the close-up).

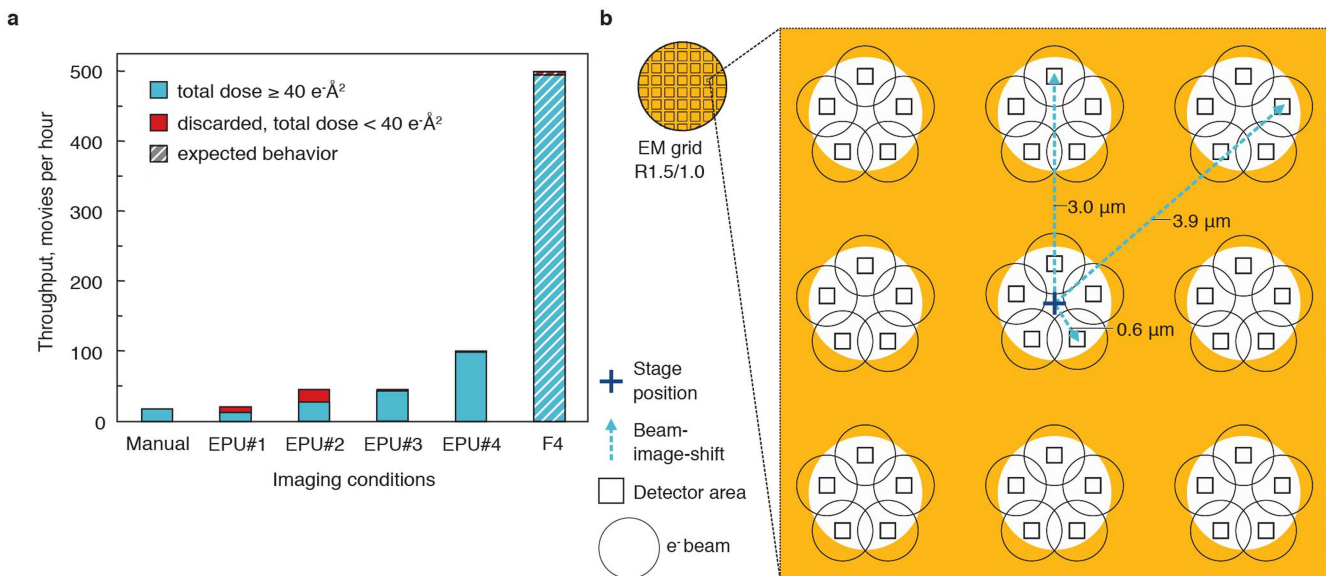
a

	Jeol 1.54 Å	Krios Mono/ BCOR 1.56 Å (COW)	Krios Mono/BCOR 1.55 Å	Krios Mono/BCOR 1.25 Å	Krios Mono/BCOR 1.33 Å	Krios Mono/BCOR 1.15 Å
Relion aberration correction	no	no	no	no	no	yes
Ewald correction	no	no	no	yes	no	yes
FSC map- model	0.87	0.86	0.864	0.88	0.897	0.851
R - overall	0.176	0.165	0.199	0.199	0.167	0.2
Cross- correlation	0.76	0.75	0.79	0.78	0.809	0.74
RMS bond length	0.022	0.016	0.015	0.024	0.0175	0.023
RMS bond angle	1.99	1.57	1.63	1.91	1.645	1.91
Build water molecules	1,375	4,172	3,140	4,200	4,330	4,622

b

Extended Data Fig. 6 | Relevant map-model building parameters and solvent molecules. **a**, As expected for such high-resolution structures, the calculated model validation parameters are in a very good range for all cryo-EM reconstructions. The results from the three structures at 1.56/1.55/1.54 Å resolution can best be compared because they were determined at very similar resolution. When comparing those structures, all validation parameters are in favour of the Krios Mono/BCOR structures. Their atomic models have better geometries and more waters were built into the maps compared to the Jeol 1.54 Å map. **b**, The number of water molecules that we localized in a structure rises with resolution of a map, which is true for X-ray and for cryo-EM. The plot

shows the number of water molecules found in the various X-ray structures (red dots) in relation to the cryo-EM maps (Relion-blue, COW-orange and Jeol-magenta). At the 1.5 Å level, substantially more water molecules were identified for both Krios Mono/BCOR reconstructions compared to the Jeol map at very similar nominal resolution. We obtained the highest number of waters for the 1.56 Å map that was calculated with the COW software. For this model, the number of built waters gets very close to the X-ray data at this resolution. It is noteworthy that the number of waters that were located in the X-ray structures is still generally higher than for the cryo-EM maps for reasons that are currently unknown.



Extended Data Fig. 7 | Improving the image acquisition speed over the time of the project. **a**, Several changes were made in the data acquisition scheme of the Titan Krios Mono/BCOR microscope. We started with manual data collection and then implemented several different EPU versions to increase the speed. EPU#1 was similar in speed to manual acquisition with one image per hole. EPU#2 required the automation of the C3 aperture and allowed us to take three images per hole. Only with EPU#3 we had a version allowing for automated re-centering of the monochromator which reduced the number of discarded images due to large dose variations. The currently highest speed in data acquisition is EPU#4 for which we reach roughly 100 movies per hour

using the recording scheme shown in **b** (only available since Dec 2019). Most data of this project was recorded with the EPU#3 scheme. **b**, To reach an acquisition speed of 100 micrographs/hour we move the stage only once to record data from 9 ice holes on a custom made EM grid (Quantifoil R1.2/1.0). Image/beam shift is applied to reach all 45 acquisition areas. The BCOR is tuned to compensate for image shift induced coma. Using this scheme we would also benefit significantly from a faster camera like the Falcon 4 (Thermo Fischer Scientific). Just by replacing the camera this would allow us to reach an almost 5 times higher recording speed of 500 micrographs per hour (**F4** in **a**).

Extended Data Table 1 | Cryo-EM data collection, refinement and validation statistics

	UVA_SCs_E (EMDB-11103) (PDB 6Z6U)	Cow (EMDB-11122) (PDB 6Z9F)	UVA (EMDB-11669) (PDB 7A6B)	UVA_SCs_B2T*_E (EMDB-11668) (PDB 7A6A)
Data collection and processing				
Magnification		120,000x		
Voltage (kV)		300		
Electron exposure (e-/Å ²)		50		
Defocus range (μm)		0.3 - 1		
Pixel size (Å)		0.492		
Symmetry imposed		O		
Initial particle images (no.)		1,470,000		
Final particle images (no.)	1,091,000	70,000	1,074,000	797,000
Map resolution (Å)	1.25	1.56	1.33	1.15
FSC threshold		0.143		
Refinement				
Initial model used (PDB code)		2CEI		
Model resolution (Å)	1.25	1.55	1.33	1.15
FSC threshold		0.5		
Model resolution range (Å)	100.02 - 1.25	100.02 - 1.55	100.02 - 1.33	100.02 - 1.15
Map sharpening B factor (Å ²)		N/A		
Model composition				
Total atoms	38,870	41,044	41,518	41,637
Water	4,200	4,172	3,854	4,622
Protein atoms	35,496	36,840	37,632	36,984
B factors (Å ²)				
Overall	23.6	34.6	27.3	22.3
R.m.s. deviations				
Bond lengths (Å)	0.024	0.016	0.018	0.023
Bond angles (°)	1.91	1.57	1.65	1.91
Validation				
MolProbity score	1.39	1.74	1.69	1.52
Clashscore	3.99	5.69	4.36	3.61
Poor rotamers (%)	1.85	3.66	4.17	3.03
Ramachandran plot				
Favored (%)	99.4	98.29	98.81	98.81
Allowed (%)	0.6	3.66	1.19	1.19
Disallowed (%)	0.00	0.00	0.00	0.00

UVA: Defocus and astigmatism correction only; COW: Defocus and astigmatism correction only, calculated with COW software; UVA_SCs_E: Defocus and astigmatism correction, scaling and Cs correction, Ewald sphere correction (final map at 1.25 Å resolution); UVA_SCs_B2T*_E: Defocus and astigmatism correction, scaling and Cs correction, higher aberration correction in image/beam shift dependent clusters, Ewald sphere correction (nominally the highest resolution map but with indications for overfitting).

Corresponding author(s): Holger Stark

Last updated by author(s): Aug 31, 2020

Reporting Summary

Nature Research wishes to improve the reproducibility of the work that we publish. This form provides structure for consistency and transparency in reporting. For further information on Nature Research policies, see [Authors & Referees](#) and the [Editorial Policy Checklist](#).

Statistics

For all statistical analyses, confirm that the following items are present in the figure legend, table legend, main text, or Methods section.

n/a Confirmed

- The exact sample size (n) for each experimental group/condition, given as a discrete number and unit of measurement
- A statement on whether measurements were taken from distinct samples or whether the same sample was measured repeatedly
- The statistical test(s) used AND whether they are one- or two-sided
Only common tests should be described solely by name; describe more complex techniques in the Methods section.
- A description of all covariates tested
- A description of any assumptions or corrections, such as tests of normality and adjustment for multiple comparisons
- A full description of the statistical parameters including central tendency (e.g. means) or other basic estimates (e.g. regression coefficient) AND variation (e.g. standard deviation) or associated estimates of uncertainty (e.g. confidence intervals)
- For null hypothesis testing, the test statistic (e.g. F , t , r) with confidence intervals, effect sizes, degrees of freedom and P value noted
Give P values as exact values whenever suitable.
- For Bayesian analysis, information on the choice of priors and Markov chain Monte Carlo settings
- For hierarchical and complex designs, identification of the appropriate level for tests and full reporting of outcomes
- Estimates of effect sizes (e.g. Cohen's d , Pearson's r), indicating how they were calculated

Our web collection on [statistics for biologists](#) contains articles on many of the points above.

Software and code

Policy information about [availability of computer code](#)

Data collection	EPU (Thermo Fisher Scientific) with modifications (v2.4.0.78 Patch-2882REL4)
Data analysis	Relion 3.1, COW (beta version), Pymol 2.3.4, MOLREP (11.7.02), Refmac5 (5.8.0258), Coot (0.8.9.2), Cinema4D R14, GCTF 1.06

For manuscripts utilizing custom algorithms or software that are central to the research but not yet described in published literature, software must be made available to editors/reviewers. We strongly encourage code deposition in a community repository (e.g. GitHub). See the Nature Research [guidelines for submitting code & software](#) for further information.

Data

Policy information about [availability of data](#)

All manuscripts must include a [data availability statement](#). This statement should provide the following information, where applicable:

- Accession codes, unique identifiers, or web links for publicly available datasets
- A list of figures that have associated raw data
- A description of any restrictions on data availability

The atomic models have been deposited in the Protein Data Bank (PDB) with the following accession codes: 1.56 Å structure (COW) 6Z9F, 1.55 Å structure 6Z9E, 1.33 Å structure 7A6B 1.25 Å structure 6Z6U, and 1.15 Å structure 7A6A. The cryo-EM maps have been deposited in the Electron Microscopy Data Bank as follows: 1.56 Å map (COW, EMD-11122), 1.55 Å map (EMD-11121), 1.33 Å map (EMD-11669), 1.25 Å map (EMD-11103) and 1.15 Å map (EMD-11168).

Field-specific reporting

Please select the one below that is the best fit for your research. If you are not sure, read the appropriate sections before making your selection.

Life sciences Behavioural & social sciences Ecological, evolutionary & environmental sciences

For a reference copy of the document with all sections, see nature.com/documents/nr-reporting-summary-flat.pdf

Life sciences study design

All studies must disclose on these points even when the disclosure is negative.

Sample size	1.466.774 particles from 10.398 movies
Data exclusions	only wrongly picked particles were excluded
Replication	data was obtained from 40 EM grids in 40 image recording sessions
Randomization	B factor determination was carried out 3 times by randomly selecting subsets of data
Blinding	blinding is not required for structure determination of one macromolecular complex

Reporting for specific materials, systems and methods

We require information from authors about some types of materials, experimental systems and methods used in many studies. Here, indicate whether each material, system or method listed is relevant to your study. If you are not sure if a list item applies to your research, read the appropriate section before selecting a response.

Materials & experimental systems

n/a	Involved in the study
<input checked="" type="checkbox"/>	<input type="checkbox"/> Antibodies
<input checked="" type="checkbox"/>	<input type="checkbox"/> Eukaryotic cell lines
<input checked="" type="checkbox"/>	<input type="checkbox"/> Palaeontology
<input checked="" type="checkbox"/>	<input type="checkbox"/> Animals and other organisms
<input checked="" type="checkbox"/>	<input type="checkbox"/> Human research participants
<input checked="" type="checkbox"/>	<input type="checkbox"/> Clinical data

Methods

n/a	Involved in the study
<input checked="" type="checkbox"/>	<input type="checkbox"/> ChIP-seq
<input checked="" type="checkbox"/>	<input type="checkbox"/> Flow cytometry
<input checked="" type="checkbox"/>	<input type="checkbox"/> MRI-based neuroimaging